

Evidence of a perpendicular magnetocrystalline anisotropy in a Mn_5Ge_3 epitaxial thin film revealed by ferromagnetic resonance

A. Truong,¹ A. O. Watanabe,¹ T. Sekiguchi,¹ P. A. Mortemousque,¹ T. Sato,² K. Ando,¹ and K. M. Itoh^{1,*}

¹*School of Fundamental Science and Technology, Keio University, 3-14-1 Hiyoshi, Kohoku-ku, Yokohama 223-8522, Japan*

²*School of Integrated Design Engineering, Keio University, 3-14-1 Hiyoshi, Kohoku-ku, Yokohama 223-8522, Japan*

(Received 28 October 2014; revised manuscript received 25 November 2014; published 10 December 2014)

A systematic study of the angular and temperature dependencies of the ferromagnetic resonance (FMR) of manganese germanide Mn_5Ge_3 grown on Ge(111) by solid phase epitaxy is reported. The FMR measurements performed in the out-of-plane geometry show that an out-of-plane anisotropy contribution exists in this material, and it increases with decreasing temperatures. However, the perpendicular magnetization curves imply that the shape anisotropy determines the orientation of the magnetization at any temperature. It is also shown that the Callen-Callen law cannot be used to describe the temperature dependence of the perpendicular anisotropy in Mn_5Ge_3 . Such temperature dependence of the magnetocrystalline anisotropy shows the invalidity of the single-ion anisotropy model for Mn_5Ge_3 .

DOI: [10.1103/PhysRevB.90.224415](https://doi.org/10.1103/PhysRevB.90.224415)

PACS number(s): 76.50.+g, 75.50.Cc, 75.30.Gw, 37.20.+j

I. INTRODUCTION

The study of group IV diluted magnetic semiconductors based on germanium (Ge) and manganese (Mn) has motivated the investigation of the magnetic properties of Mn-rich Mn-Ge compounds. Park *et al.* (Ref. [1]) succeeded in distributing Mn in a Ge semiconductor matrix at low Mn concentrations (below 8%). The Curie temperature did not, however, exceed 120 K. It has also been shown [2,3] that when the Mn concentration x exceeds a few percent, $\text{Ge}_{1-x}\text{Mn}_x$ tends to undergo a phase separation, due to the low solubility of Mn in Ge, leading to the formation of Mn-rich clusters, which are thermodynamically more stable than the Mn-diluted compound. Manganese germanide, in the form of Mn_5Ge_3 , has recently drawn attention due to its potential for spin injection and spintronics applications [4–7]. It has been shown that Mn-Ge can be grown epitaxially on a Ge(111) substrate and form a stoichiometric Mn_5Ge_3 crystal, by using the solid phase epitaxy method [8–13]. Indeed, an epitaxial relationship has been revealed between $\text{Mn}_5\text{Ge}_3(001)$ and Ge(111) (Refs. [12,14]). Studies of the thermal stability of the Mn_5Ge_3 compound led to the conclusion that epitaxial Mn_5Ge_3 can be formed by solid phase epitaxy on Ge(111) for growth temperatures between 300 °C and 650 °C. The Mn would leave the Ge(111) surface if the temperature is excessively high [8]. The Curie temperature T_C of such material is measured to be 296 K for the bulk material [8] and can be equal to or slightly higher than 296 K in the form of thin films depending on the growth methods [15], and can be increased to 430 K by carbon doping [14]. This material is therefore a potential candidate for room temperature magnetic applications.

In ferromagnetic materials, the magnetocrystalline anisotropy usually shows a dependence on temperature [16–19]. For practical applications, it is therefore important to determine the behavior of the magnetocrystalline anisotropy in a wide temperature range, especially when the ferromagnet is intended to be used at a specific temperature range. While the

temperature dependence of the magnetocrystalline anisotropy for ferromagnets with localized magnetic moments can be described quite well by the Callen-Callen law [16,17], which is based on a single-ion anisotropy model, there are ferromagnetic transition-metal alloys that can show more complicated behaviors [17,18]. In this paper, we show the presence of magnetocrystalline anisotropy in a Mn_5Ge_3 thin film, in addition to the shape anisotropy. Section II deals with the sample's growth method and structural characterization. Section III shows the results of the measurements of magnetic properties. The in-plane magnetization curves show a decreasing remanence ratio with decreasing temperature. Furthermore, we report the presence of perpendicular anisotropy, whose contribution increases when the temperature decreases. We also discuss the invalidity of the Callen-Callen law for our Mn_5Ge_3 thin film.

II. SAMPLE PREPARATION

The sample was grown by using the molecular beam epitaxy (MBE) technique, at a base pressure lower than 8×10^{-8} Pa. The quality of the sample's surface was monitored *in situ* by reflection high-energy electron diffraction (RHEED), in both $[1\bar{1}0]$ and $[11\bar{2}]$ directions of the Ge(111) substrate. The sample's internal structure was observed *ex situ* by transmission electron microscopy (TEM).

The substrate was degassed at 600 °C for 2 h. A Ge buffer layer was grown on the Ge(111) substrate at a substrate temperature T_{sub} of 600 °C, in order to keep a good crystallinity. An annealing at 700 °C for 1 h followed by a cooling below 200 °C resulted in the well-known $c(2 \times 8)$ reconstruction of the clean Ge(111) surface [Figs. 1(a) and 1(b)]. Mn was then deposited on this $c(2 \times 8)$ surface at $T_{\text{sub}} = 40$ °C. The RHEED patterns during the growth of the Mn layer revealed a three-dimensional growth, characterized by the presence of transmission spots [Figs. 1(c) and 1(d)]. A solid-state reaction between manganese and germanium was activated by annealing the sample at 450 °C for 15 min, leading to the $\sqrt{3} \times \sqrt{3}$ reconstruction, indicating the (001) surface of Mn_5Ge_3 [Figs. 1(e) and 1(f)]. In order to prevent the

*kitoh@appi.keio.ac.jp

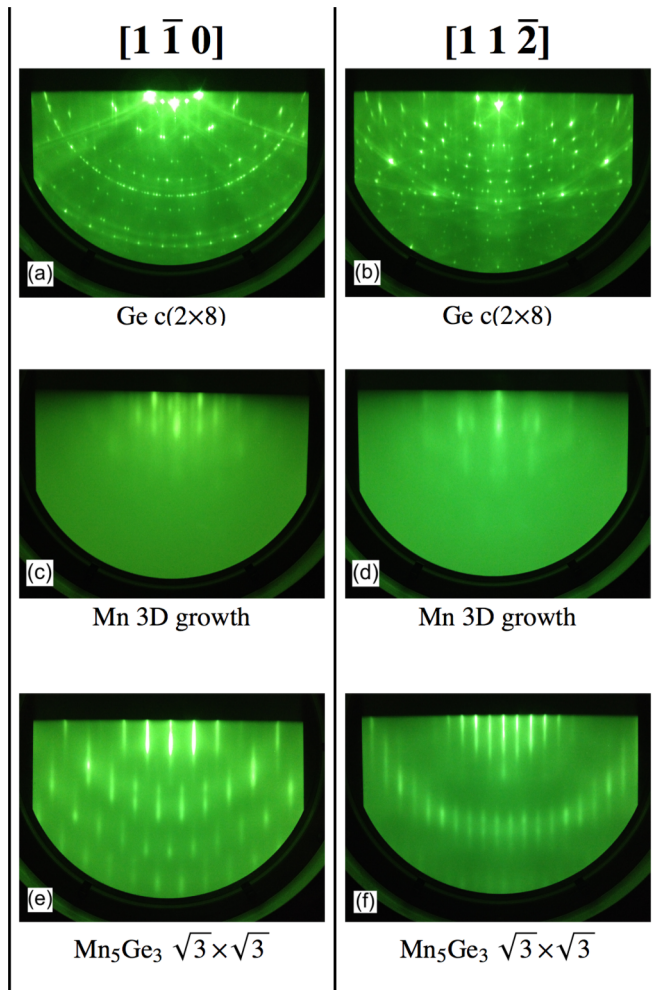


FIG. 1. (Color online) RHEED patterns in the $[1\bar{1}0]$ and $[11\bar{2}]$ directions of the Ge(111) substrate, with an acceleration energy of 12 keV, at different steps of the growth: (a) and (b) the $c(2 \times 8)$ reconstructed surface of Ge buffer layer; (c) and (d) transmission patterns after the growth of the Mn layer; (e) and (f) the $\sqrt{3} \times \sqrt{3}$ structure of Mn_5Ge_3 after the solid state reaction.

manganese germanide layer from oxidizing, which is crucial to keep its magnetic properties, an amorphous Ge capping layer was grown with a low growth temperature so that the segregation of Mn_5Ge_3 to the surface is suppressed. Such segregation was demonstrated in Ref. [20]. The thickness of the deposited Mn layer was 22 nm. During the post-Mn-deposition annealing, a part of the Ge buffer layer was consumed for the solid-state growth to form a 30-nm-thick Mn_5Ge_3 layer. In order to confirm the crystallographic structure of our sample, x-ray diffraction (XRD) patterns were measured by performing θ - 2θ scans on the thin film. A pure Ge(111) substrate was also measured by XRD, as a reference sample. In the obtained XRD spectra shown in Fig. 2, we identified the peaks from the Ge(111) substrate and the $\text{Mn}_5\text{Ge}_3(001)$ film, which are consistent with the results obtained in previous studies [8,21]. According to this XRD spectrum, the lattice parameters were $a(\text{Ge}) = 5.664 \text{ \AA}$ for the cubic Ge, consistent with the value found in literature [22], and $c(\text{Mn}_5\text{Ge}_3) = 5.057 \text{ \AA}$ for the hexagonal Mn_5Ge_3 . The hexagonal basal plane lattice

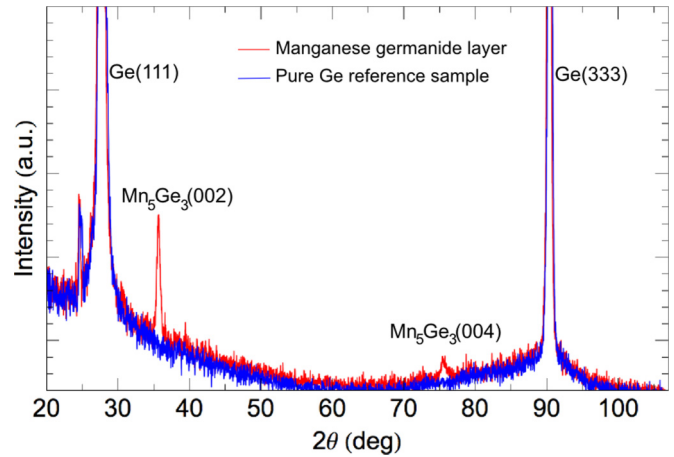


FIG. 2. (Color online) An x-ray diffraction spectrum for the MBE-grown Mn_5Ge_3 thin film (red curve), using $\text{Cu } K\alpha$ radiation (wavelength $\lambda = 0.15418 \text{ nm}$). A pure Ge substrate has also been measured and serves as a reference (blue curve). The peak at $2\theta = 24.6^\circ$ corresponds to a signal coming from the germanium irradiated by $\text{Cu } K\beta$ radiation originating from the x-ray source.

parameter of Mn_5Ge_3 was evaluated to be $a(\text{Mn}_5\text{Ge}_3) = 7.112 \text{ \AA}$, by using an off-normal angle XRD measurement (not shown here). The unit-cell parameters of the Mn_5Ge_3 film measured in this work are close to the values found for the bulk [23] and consistent with the previous work on thin films [15]. Energy dispersive x-ray (EDX) measurements of the Mn-Ge layer showed a Mn:Ge composition of 62%:38%, which corresponds to the stoichiometry in Mn_5Ge_3 . The homogeneity of the composition was confirmed by performing EDX measurements at many random locations in the manganese germanide layer. The cross-sectional TEM images in Fig. 3 show the structure of the Mn_5Ge_3 thin film on the Ge(111) buffer layer. One can see that the growth is epitaxial, with no clusters and the interfaces are relatively smooth.

Moreover, we have found that Mn_5Ge_3 always forms coherently on Ge(111), with its hexagonal $[010]$ in-plane direction always being parallel to the cubic $[11\bar{2}]$ in-plane direction of the Ge substrate. This, we believe, is due to the fact that the in-plane atomic spacing 7.112 \AA in the $[010]$

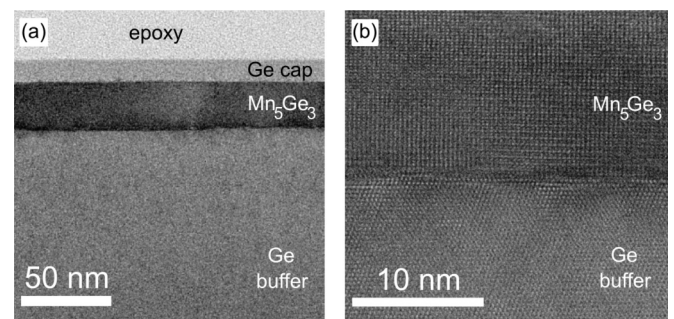


FIG. 3. Cross-sectional TEM images of the epitaxial Mn_5Ge_3 layer. (a) An overview of the structure shows relatively smooth interfaces. (b) A close-up view on the $\text{Mn}_5\text{Ge}_3/\text{Ge}$ interface shows the epitaxial growth of $\text{Mn}_5\text{Ge}_3(001)$ on Ge(111).

direction of Mn_5Ge_3 is about the same as the in-plane atomic spacing 6.937 Å in the $[11\bar{2}]$ direction of Ge.

III. STUDY OF MAGNETIC PROPERTIES

A. Measurement of magnetic properties by SQUID

The magnetic properties of the Mn_5Ge_3 thin film are measured by superconducting quantum interference device (SQUID) magnetometry with a magnetic field applied in the sample's plane. The magnetization hysteresis curves at different temperatures for the Mn_5Ge_3 thin film are shown in Fig. 4. One can notice that the shape of the magnetic hysteresis undergoes a change depending on the temperature. For temperatures closer to the Curie point, the hysteresis of the in-plane magnetization is close to having a square shape [Fig. 4(a)], indicating that the magnetization easy axis and the field axis are close to perfect parallel alignment at zero field. On the other hand, when the temperature is decreased, the magnetization curve loses its square shape and the remanence to saturation magnetization ratio decreases, going from $M_R/M_S \simeq 0.85$ at 290 K to $M_R/M_S \simeq 0.25$ below 200 K [Figs. 4(b)–4(e)]. The magnetization hysteresis cycle is partly ruled by the competition between the anisotropy energy and the exchange interaction energy, possibly resulting

in magnetic domains. The remanence ratio is dependent on the anisotropy energy to exchange energy ratio [24] and also on the competition between several magnetic anisotropies [25]. Since the sample is a thin film, the shape anisotropy is the dominant form of magnetic anisotropy, and keeps the magnetization in the sample's plane. However, the presence of magnetocrystalline anisotropy, in addition to the shape anisotropy, could reduce the in-plane magnetization at low fields. In Fig. 4(a), it appears that an infinitesimal field variation is required to switch and saturate the magnetization, while a much higher field is required at temperatures lower than 200 K [Figs. 4(b)–4(e)], with saturation fields equal to 0.037 T at 290 K, 0.11 T at 100 K, 0.16 T at 30 K, and 0.44 T at 5 K. Moreover, while the in-plane remanence ratio seems to undergo a strong variation between 290 and 200 K, it remains relatively constant in the whole temperature range below 200 K. The temperature dependence of the shape anisotropy energy is the same as that of the square magnetization. Since Mn_5Ge_3 has a hexagonal crystal lattice, one can assume that the hexagonal c axis could give a contribution to the magnetocrystalline anisotropy even in a thin film. So, if such magnetocrystalline anisotropy exists, its contribution would increase faster than the shape anisotropy with decreasing temperature, thus decreasing the in-plane remanence ratio at low temperatures and having no visible effects at temperatures close to T_c . In order to study the effects of an out-of-plane uniaxial magnetocrystalline anisotropy, the perpendicular magnetization curves have been measured [the magnetization curve at 30 K is plotted in Fig. 4(f)] and show a remanence ratio close to zero and a saturation field higher than in the in-plane curves, so such out-of-plane anisotropy would be too weak to orientate the magnetization along the perpendicular axis, but could still contribute to lowering the remanence ratio in the in-plane magnetization curves. Therefore, in order to have a better understanding of the decrease in remanence ratio at low temperature, ferromagnetic resonance measurements are carried out to determine the presence and intensity of the out-of-plane anisotropy.

We also use the SQUID magnetometry to measure the saturation magnetization at different temperatures (see Fig. 5),

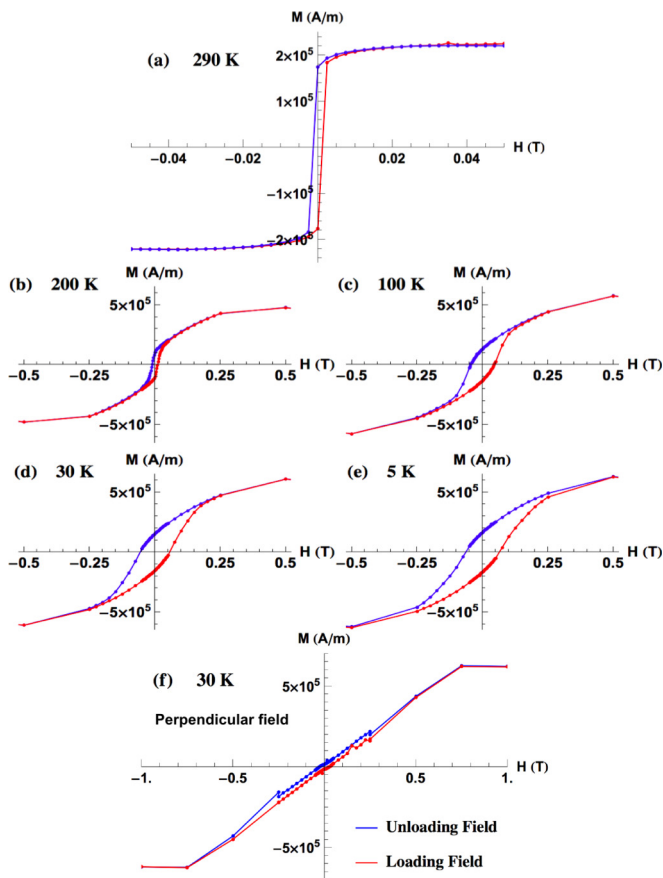


FIG. 4. (Color online) Magnetization as a function of the applied magnetic field at (a) 290 K, (b) 200 K, (c) 100 K, (d) 30 K, and (e) 5 K. The field is applied in the sample's plane for (a)–(e). In (f), the field is applied in the sample's normal axis and the measurement temperature is 30 K. Note the different scales in (a) and (f).

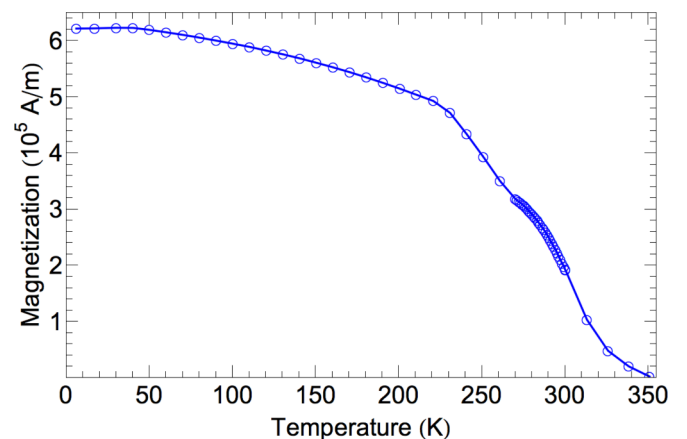


FIG. 5. (Color online) Saturation magnetization versus temperature curve of the MBE-grown Mn_5Ge_3 thin film, measured by SQUID, using an external field of 1.5 T. The Curie temperature is $T_c = 300 \pm 5$ K.

which will be useful for the temperature-dependent ferromagnetic resonance (FMR) measurements in the following section.

B. Theoretical model for ferromagnetic resonance in Mn_5Ge_3

The ferromagnetic resonance technique is an efficient way to determine the properties related to the magnetocrystalline anisotropy of magnetic materials [26–29]. Each type of crystal symmetry is defined by a free energy and the magnetization easy axis is found by minimizing this free energy. The crystalline structure of Mn_5Ge_3 has a hexagonal symmetry, therefore, the corresponding free energy will have the same expression as in the case of a tetragonal structure, except that the fourth and sixth order anisotropy terms are neglected, thus only leaving second order terms. The total free energy includes three contributions [26], which are the Zeeman energy $F_{\text{Zeeman}} = -HM[\cos\theta_M \cos\theta_H + \sin\theta_M \sin\theta_H \cos(\varphi_M - \varphi_H)]$, the shape anisotropy energy $F_{\text{shape}} = 2\pi M^2 \cos^2\theta_M$ considering that the thin film is an infinite plane, and the magnetocrystalline anisotropy energy. H and M are the amplitudes of the external magnetic field and the magnetization of the sample, respectively. The coordinate system used in this study and the angles $\theta_M, \theta_H, \varphi_M$, and φ_H are defined in Fig. 6. Since a hexagonal symmetry is considered in our case, the magnetocrystalline anisotropy energy is only parametrized by H_{\parallel} and H_{\perp} , the second order in-plane and out-of-plane anisotropy fields, respectively. Therefore, the free energy of our sample is expressed as follows:

$$F_{\text{hexagonal}} = F_{\text{Zeeman}} + F_{\text{shape}} - \frac{1}{2}MH_{\perp} \cos^2\theta_M - \frac{1}{2}MH_{\parallel} \sin^2\theta_M \cos^2\left(\varphi_M - \frac{\pi}{3}\right). \quad (1)$$

In a ferromagnetic material, the magnetization dynamics $\mathbf{M}(t)$ can be modeled by the Landau-Lifshitz-Gilbert (LLG)

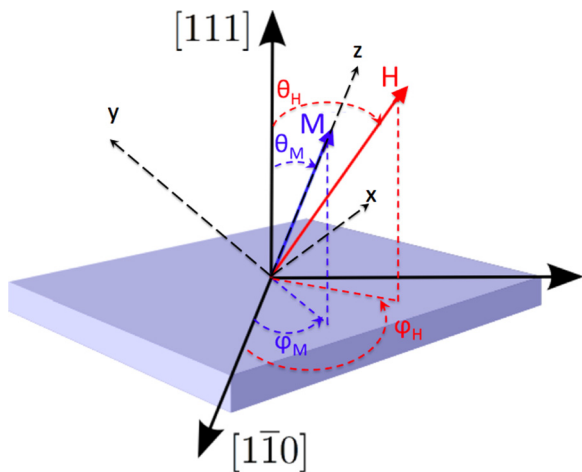


FIG. 6. (Color online) Coordinate system used for the FMR calculations and experiments. θ_M and θ_H are the out-of-plane magnetization angle and field angle, respectively. And φ_M and φ_H are the in-plane magnetization angle and field angle, respectively. The sample's normal axis corresponds to the $[111]$ direction of the Ge substrate, and (x, y, z) is defined so that the z direction is parallel to the magnetization.

equation:

$$\frac{d\mathbf{M}(t)}{dt} = -\gamma\mathbf{M}(t) \times \mathbf{H}_{\text{eff}} + \frac{\alpha}{M_S}\mathbf{M}(t) \times \frac{d\mathbf{M}(t)}{dt}, \quad (2)$$

where γ is the gyromagnetic ratio, α is the damping constant, and M_S is the saturation magnetization. Only the first term is required to study the angular dependence of the resonance field. The second term, which involves the damping constant, is related to the angular dependence of the linewidth of the FMR signals.

The effective magnetic field \mathbf{H}_{eff} includes the external magnetic field \mathbf{H} and a field \mathbf{H}_M , which takes into account the contributions of the perpendicular anisotropy H_{\perp} and the demagnetizing field induced by the magnetization $\mathbf{M}(t)$. Since the demagnetizing field and the perpendicular anisotropy field have the same symmetry, it is natural to include them in the same contribution. The ferromagnetic resonance condition is derived from the total free energy and the LLG equation, and is given by

$$\left(\frac{\omega}{\gamma}\right)^2 = [H_{\text{FMR}a_1} + b_1][H_{\text{FMR}a_1} + b_2] - b_3^2, \quad (3)$$

where ω is the microwave frequency, and a_1, b_1, b_2 , and b_3 are given by

$$a_1 = \cos\theta_M \cos\theta_H + \sin\theta_M \sin\theta_H \cos(\varphi_M - \varphi_H),$$

$$b_1 = -\left[4\pi M_S - H_{\perp} + H_{\parallel} \cos^2\left(\varphi_M - \frac{\pi}{3}\right)\right] \cos(2\theta_M),$$

$$b_2 = -(4\pi M_S - H_{\perp}) \cos^2\theta_M$$

$$-H_{\parallel} \left\{ \left[\cos\theta_M \cos\left(\varphi_M - \frac{\pi}{3}\right) \right]^2 - \cos 2\left(\varphi_M - \frac{\pi}{3}\right) \right\},$$

$$b_3 = H_{\parallel} \cos\theta_M \sin\left(\varphi_M - \frac{\pi}{3}\right) \cos\left(\varphi_M - \frac{\pi}{3}\right).$$

In the following section, the temperature dependence of the magnetocrystalline anisotropy in our sample will be discussed. The Callen-Callen law is a theory derived from models developed by Akulov [30] and Zener [31,32], which assumes that the variations of the anisotropy energy as a function of the temperature have the same origins as that of the magnetization, due to the coupling between the magnetization and the crystal lattice. So the anisotropy coefficient can be expressed as a power law of the magnetization [30–34], as follows:

$$\left(\frac{K_n(T)}{K_n(0)}\right) = \left(\frac{M_S(T)}{M_S(0)}\right)^{n(n+1)/2}, \quad (4)$$

where $K_n(T)$ and $M_S(T)$ are the n th order anisotropy coefficient at temperature T and the saturation magnetization at temperature T , respectively. In the case of our Mn_5Ge_3 thin film, the Callen-Callen law would give a cubic law, due to the presence of a second order uniaxial anisotropy only.

C. Experimental results of FMR measurements and discussion

The experimental study of the magnetocrystalline anisotropy of Mn_5Ge_3 is carried out by using both FMR and SQUID. The dependence of the FMR signals as a function of the magnetic field angle is studied both in the in-plane and the out-of-plane geometries. The FMR measurements

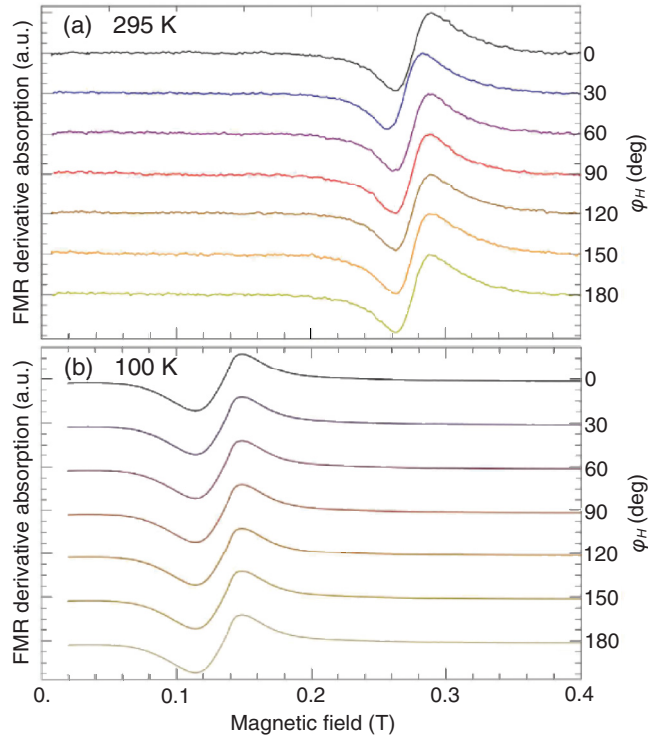


FIG. 7. (Color online) FMR signals recorded as the first derivative of the microwave absorption in the in-plane geometry at (a) 295 K and (b) 100 K. The in-plane measurements show no variation of resonance field as a function of angle, so magnetocrystalline anisotropy is absent in the sample's plane. The in-plane FMR measurements were performed by applying a magnetic field in the sample's plane and rotating it along its normal axis.

are performed by using an electron paramagnetic resonance spectrometer at a microwave frequency of 9.08 GHz. Our study focuses on the position of the ferromagnetic resonance field (H_{FMR}) as a function of the field angle at various temperatures from 18 to 295 K. The sample is rotated with a goniometer attached to the sample holder.

The in-plane FMR spectra at 295 and 100 K (Fig. 7) do not show any variations as a function of angle. Consequently, all the axes contained in the magnetic film's plane are equivalent in terms of magnetocrystalline anisotropy. All the measurements at temperatures between 18 and 295 K also lead to the same conclusion. Therefore, through those experimental measurements we can infer that the sample's plane has no magnetocrystalline anisotropy, thus resulting in $H_{\parallel} = 0$. This result is important for the out-of-plane FMR measurements because it significantly simplifies the ferromagnetic resonance condition and also results in $\varphi_M = \varphi_H$. The effective field is defined as $\mathbf{H}_{\text{eff}} = \mathbf{H} + \mathbf{H}_M$ and can be expressed in the (x, y, z) coordinate system, where

$$\mathbf{H} = H \begin{pmatrix} 0 \\ \sin(\theta_M - \theta_H) \\ \cos(\theta_M - \theta_H) \end{pmatrix}, \quad (5)$$

$$\mathbf{H}_M = -(4\pi M_S - H_{\perp}) \cos \theta_M \begin{pmatrix} 0 \\ \sin \theta_M \\ \cos \theta_M \end{pmatrix}. \quad (6)$$

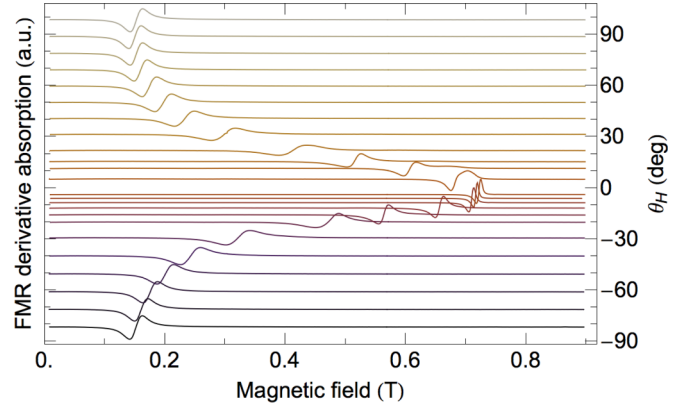


FIG. 8. (Color online) FMR spectra in the out-of-plane geometry for the Mn_5Ge_3 thin film, measured at 200 K. One can see that a higher external magnetic field is required in order to obtain the resonance as the direction of the field gets closer to the normal axis of the sample.

The out-of-plane field angle dependence of the ferromagnetic resonance field is obtained from the static equilibrium condition $\mathbf{M} \times \mathbf{H}_{\text{eff}} = \mathbf{0}$, and the ferromagnetic resonance condition. Those two conditions lead to the following set of equations:

$$2H \sin(\theta_H - \theta_M) + 4\pi M_{\text{eff}} \sin 2\theta_M = 0, \quad (7)$$

$$\left(\frac{\omega}{\gamma}\right)^2 = [H_{\text{FMR}} \cos(\theta_H - \theta_M) - 4\pi M_{\text{eff}} \cos(2\theta_M)]$$

$$\times [H_{\text{FMR}} \cos(\theta_H - \theta_M) - 4\pi M_{\text{eff}} \cos^2 \theta_M],$$

where $4\pi M_{\text{eff}} = 4\pi M_S - H_{\perp}$ is the effective magnetization.

According to the above-mentioned model, since the sample has no in-plane magnetocrystalline anisotropy, the only possible form of magnetocrystalline anisotropy is a uniaxial perpendicular anisotropy. Concerning the out-of-plane FMR measurements (Fig. 8), the presence of the demagnetizing field makes it difficult to distinguish the contribution of the perpendicular uniaxial anisotropy from that of the demagnetizing field regarding the shift of the resonance field position, when the direction of the field approaches the sample plane's normal axis. For that reason, the values of $4\pi M_{\text{eff}}$ obtained by FMR are compared with the values of $4\pi M_S$ obtained by SQUID in the previous section. A difference between the two magnetizations will show the presence of a perpendicular anisotropy.

The angular dependencies of the out-of-plane ferromagnetic resonance fields are shown in Fig. 9. One can see that, for each temperature, there is a match between the experimental angular dependence of H_{FMR} and the solutions of the set of equations (7). Solving those equations allowed us to obtain the effective magnetization for each temperature. The numerical values of effective magnetization and saturation magnetization are summarized in Table I. The experimental anisotropy coefficients are plotted as a function of temperature along with the theoretical behavior predicted by the Callen-Callen law [Eq. (4)] in Fig. 10 (red curve). We can clearly notice that the anisotropy coefficients obtained by FMR deviate from the cubic magnetization law for almost the entire temperature range. Therefore, the Callen-Callen law is not applicable to our

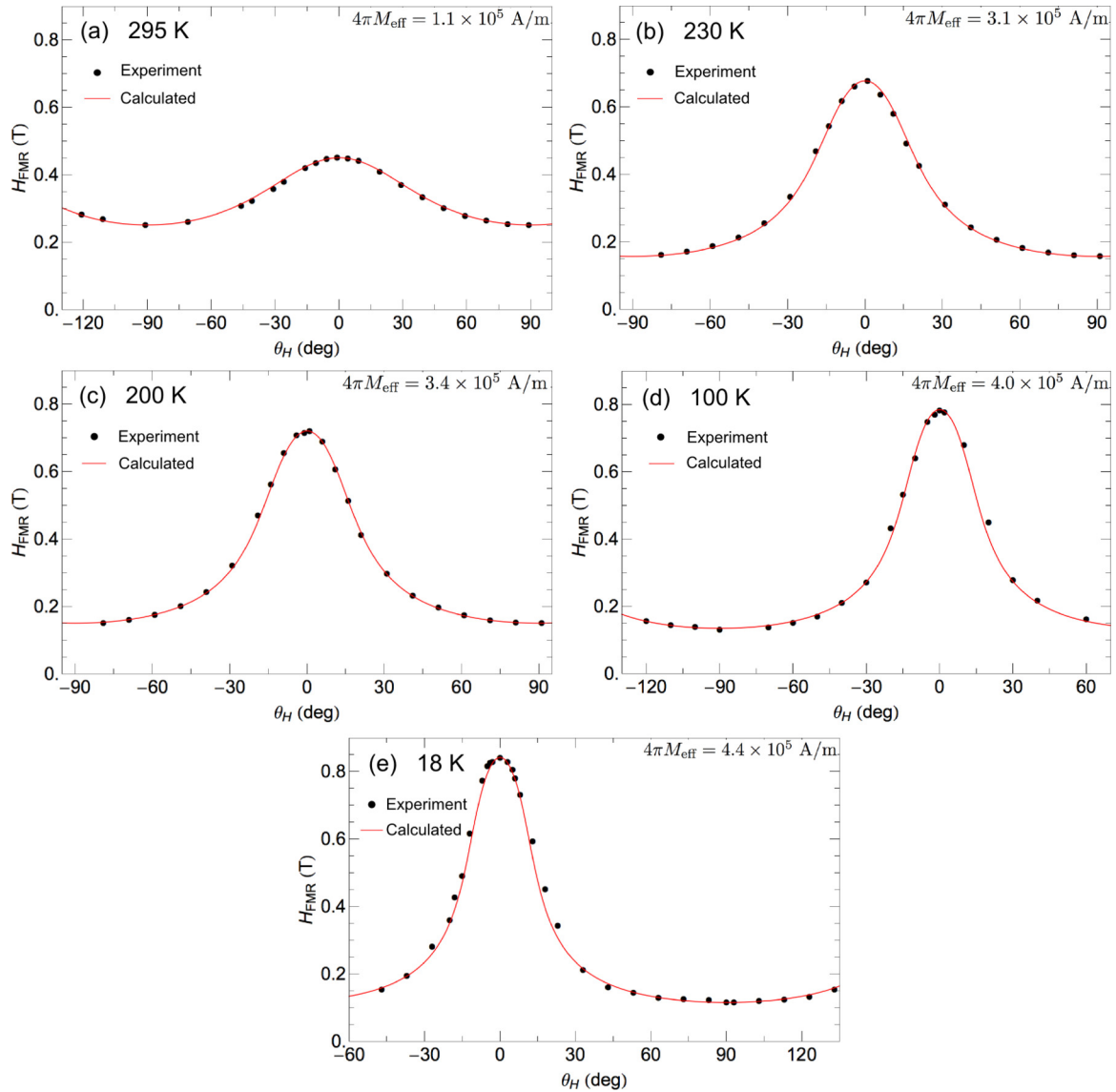


FIG. 9. (Color online) Resonance field as a function of the field angle to the normal axis of the sample for different temperatures. The experimental data is given by the black dots and the solutions of the set of equations (7) are given by the red curves. The effective magnetizations at each temperature are calculated from the above-mentioned model. The theoretical model for FMR in Mn_5Ge_3 fits well the experimental measurements.

case. However, although a cubic law is not valid for Mn_5Ge_3 , the experimental points seem to vary as the cubic square root of

TABLE I. Comparison between the saturation magnetization obtained by SQUID and the effective magnetization obtained by FMR. The perpendicular anisotropy field is calculated by subtracting the two magnetizations. K_{\perp} is deduced from $H_{\perp} = 2K_{\perp}/M_S$.

T (K)	$4\pi M_{eff}$ (A/m)	$4\pi M_S$ (A/m)	H_{\perp} (A/m)	K_{\perp} (A ² /m ²)
18	4.4×10^5	6.2×10^5	1.8×10^5	5.6×10^{10}
100	4.0×10^5	5.8×10^5	1.8×10^5	5.2×10^{10}
200	3.4×10^5	5.1×10^5	1.7×10^5	4.3×10^{10}
230	3.1×10^5	4.7×10^5	1.6×10^5	3.8×10^{10}
295	1.1×10^5	2.2×10^5	1.1×10^5	1.2×10^{10}

the magnetization. A relatively good fit with the corresponding curve can be seen in Fig. 10 (blue curve). The red and blue curves in Fig. 10 are calculated from the temperature dependence of the magnetization measured by SQUID in Fig. 5. In ferromagnets, the magnetocrystalline anisotropy usually decreases much faster than the magnetization when the temperature increases, with exponents equal to 10 or 21 for cubic anisotropies and 3 for uniaxial anisotropy [31–35]. In our case, the perpendicular anisotropy energy still decreases faster than the magnetization but at a slower pace than what can be found in literature. According to Eq. (1) and the result deduced from Fig. 10, the perpendicular anisotropy energy can be written as

$$F_{\perp} = K_{\perp}(18 \text{ K}) \left(\frac{M_S(T)}{M_S(18 \text{ K})} \right)^{1.5} \cos^2 \theta_M. \quad (8)$$

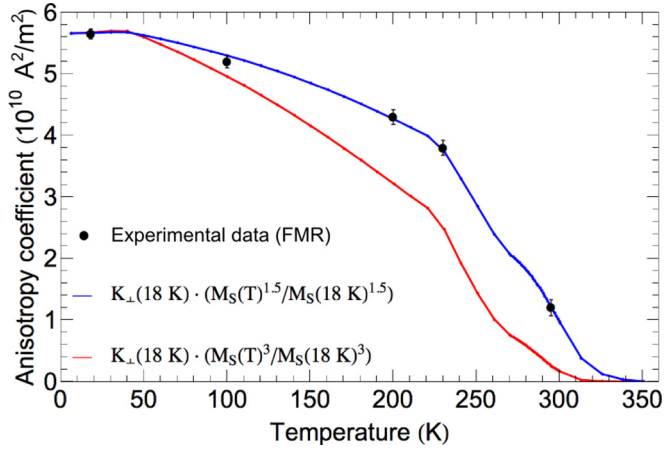


FIG. 10. (Color online) The red curve represents the calculated prediction from the Callen-Callen law for a second order uniaxial anisotropy, and the blue curve represents the calculated temperature dependence of the anisotropy energy coefficient assuming that it varies as the cubic square root of the magnetization. The calculations are based on the results given in Fig. 5. A cubic square root law seems to be more adapted to describe magnetocrystalline anisotropy in Mn_5Ge_3 than the cubic relationship predicted by the Callen-Callen law. The Callen-Callen law appears to be valid only at low temperatures (< 40 K).

As a result, the temperature dependence of the perpendicular anisotropy to shape anisotropy energy ratio is given by the following relationship:

$$\frac{F_{\perp}}{F_{\text{shape}}} \propto \frac{1}{\sqrt{M_S(T)}}. \quad (9)$$

Such temperature dependence shows that the contribution of the perpendicular anisotropy actually becomes a lot weaker than that of the shape anisotropy when the temperature decreases. Consequently, although the presence of a perpendicular magnetocrystalline anisotropy has been evidenced by FMR, it does not explain why the in-plane remanence ratio of the Mn_5Ge_3 thin film decreases at low temperatures. We can thus infer that the decrease of the in-plane remanence ratio has another origin, such as the variation of the strain in the Mn_5Ge_3 crystal with temperature.

Even though the perpendicular anisotropy is not the direct cause of the decrease of the in-plane remanent magnetization, its temperature dependence shows interesting and unusual features. It has been reported that the temperature dependence of the magnetocrystalline anisotropy given by the Callen-Callen law represents a relatively good model for ferromagnets with localized magnetic moments [36]. This is because it is based on a single-ion anisotropy model. In our case, the perpendicular uniaxial anisotropy still follows a power law, but the power is lower than the predicted value. Being a compound based on a transition metal, Mn_5Ge_3 is likely to be an itinerant ferromagnet, and the Callen-Callen law may be less accurate for magnetocrystalline anisotropy in itinerant ferromagnets. It has been established in a previous study that itinerant ferromagnetism can induce a decrease of the exponent in the power law [36], and this fact has mainly been reported for the case of the $L1_0$ phase of FePt, for which the exponent

in the temperature dependence is 2.1 instead of 3 for the uniaxial anisotropy [36–38]. Such temperature dependence has successfully been modeled by using a relativistic description of the electronic structures, which gives a better description of the spin-orbit interaction [37,38]. The application of such model to our case may not be straightforward due to the complex stoichiometry of Mn_5Ge_3 and the origin of its ferromagnetism not being fully understood. So, although we can assume that the deviation from the Callen-Callen law in our case is due to itinerant ferromagnetism, the reason why the exponent is decreased from 3 to 1.5 remains to be studied more thoroughly. And one should also note that the assumptions made in the Callen-Callen model do not take into account the magnetostriction [33,34]. When the temperature varies, the c/a ratio of the hexagonal Mn_5Ge_3 can also change and lead to the presence of magnetostriction, which represents a magnetic anisotropy that is intrinsic to the material. Further investigations will be carried out to verify if magnetostriction, along with the itinerant nature of the ferromagnetism in Mn_5Ge_3 , can be the reason why the temperature dependence of its perpendicular uniaxial anisotropy deviates from the Callen-Callen law.

IV. SUMMARY AND CONCLUSION

In summary, the use of SQUID magnetization measurements and FMR measurements together allowed us to detect the presence of a perpendicular magnetic anisotropy in a Mn_5Ge_3 thin film, which increases when the temperature decreases. We successfully estimated the numerical values of the anisotropy fields for several temperatures, and it is clear that the temperature dependence of the perpendicular anisotropy does not follow the Callen-Callen law in the case of this material. Its variation pattern appears to be closer to the cubic square root of the magnetization, and 1.5 is an unusual scaling exponent for a case of uniaxial anisotropy. Such temperature dependence would mean that the perpendicular anisotropy in Mn_5Ge_3 does not contribute to the loss of the in-plane magnetic remanence ratio at low temperatures, as assumed initially. Knowing that the c axis of Mn_5Ge_3 is the preferential axis for the magnetization in the bulk material, the presence of such perpendicular anisotropy in the thin film is most likely due to the particular epitaxial relationship between the ferromagnet and the substrate $\text{Mn}_5\text{Ge}_3(001)/\text{Ge}(111)$, which allows the hexagonal c axis to grow perpendicularly to the substrate, thus giving rise to a magnetocrystalline anisotropy in the normal axis of the thin film, in addition to the shape anisotropy. The temperature dependence of magnetocrystalline anisotropy stressed in this work represents another case of noninteger power law of magnetization, in addition to the studies done on $L1_0$ phases in the past.

ACKNOWLEDGMENTS

This work was supported in part by the Grant-in-Aid for Scientific Research by MEXT, in part by NanoQuine, and in part by JSPS Core-to-Core Program.

- [1] Y. D. Park, A. T. Hanbicki, S. C. Erwin, C. S. Hellberg, J. M. Sullivan, J. E. Mattson, T. F. Ambrose, A. Wilson, G. Spanos, and B. T. Jonker, *Science* **295**, 651 (2002).
- [2] R. Gunnella, L. Morresi, N. Pinto, A. Di Cicco, L. Ottaviano, M. Passacantando, A. Verna, G. Impellizzeri, A. Irrera, and F. d'Acapito, *J. Phys.: Condens. Matter* **22**, 216006 (2010).
- [3] C. Bihler, C. Jaeger, T. Vallaitis, M. Gjukic, M. S. Brandt, E. Pippel, J. Woltersdorf, and U. Gösele, *Appl. Phys. Lett.* **88**, 112506 (2006).
- [4] S. Picozzi, A. Continenza, and A. J. Freeman, *Phys. Rev. B* **70**, 235205 (2004).
- [5] S. A. Wolf, D. D. Awschalom, R. A. Buhrman, J. M. Daughton, S. von Molnár, M. L. Roukes, A. Y. Chtchelkanova, and D. M. Treger, *Science* **294**, 1488 (2001).
- [6] R. P. Panguluri, C. Zeng, H. H. Weitering, J. M. Sullivan, S. C. Erwin, and B. Nadgorny, *Phys. Status Solidi B* **242**, R67 (2005).
- [7] J. Tang, C. Y. Wang, L. T. Chang, Y. Fan, T. Nie, M. Chan, W. Jiang, Y. T. Chen, H. J. Yang, H. Y. Tuan, L. J. Chen, and K. L. Wang, *Nano Lett.* **13**, 4036 (2013).
- [8] C. Zeng, S. C. Erwin, L. C. Feldman, A. P. Li, R. Jin, Y. Song, J. R. Thompson, and H. H. Weitering, *Appl. Phys. Lett.* **83**, 5002 (2003).
- [9] C. Zeng, W. Zhu, S. C. Erwin, Z. Zhang, and H. H. Weitering, *Phys. Rev. B* **70**, 205340 (2004).
- [10] L. Sangaletti, D. Ghidoni, S. Pagliara, A. Goldoni, A. Morgante, L. Floreano, A. Cossaro, M. C. Mozzati, and C. B. Azzoni, *Phys. Rev. B* **72**, 035434 (2005).
- [11] L. Sangaletti, E. Magnano, F. Bondino, C. Cepek, A. Sepe, and A. Goldoni, *Phys. Rev. B* **75**, 153311 (2007).
- [12] S. Olive-Mendez, A. Spiesser, L. A. Michez, V. Le Thanh, A. Glachant, J. Derrien, T. Devillers, A. Barski, and M. Jamet, *Thin Solid Films* **517**, 191 (2008).
- [13] J. Hirvonen Grytzeli, H. M. Zhang, and L. S. O. Johansson, *Phys. Rev. B* **86**, 125313 (2012).
- [14] A. Spiesser, I. Slipukhina, M. T. Dau, E. Arras, V. Le Thanh, L. Michez, P. Pochet, H. Saito, S. Yuasa, M. Jamet, and J. Derrien, *Phys. Rev. B* **84**, 165203 (2011).
- [15] A. Spiesser, S. F. Olive-Mendez, M. T. Dau, L. A. Michez, A. Watanabe, V. Le Thanh, A. Glachant, J. Derrien, A. Barski, and M. Jamet, *Thin Solid Films* **518**, S113 (2010).
- [16] H. B. Callen and E. Callen, *J. Phys. Chem. Solids* **27**, 1271 (1966).
- [17] E. R. Callen and H. B. Callen, *Phys. Rev.* **129**, 578 (1963).
- [18] R. Skomski, O. N. Mryasov, J. Zhou, and D. J. Sellmyer, *J. Appl. Phys.* **99**, 08E916 (2006).
- [19] J. F. Herbst, *Rev. Mod. Phys.* **63**, 819 (1991).
- [20] M. T. Dau, V. Le Thanh, L. A. Michez, M. Petit, T. G. Le, O. Abbes, A. Spiesser, and A. Ranguis, *New J. Phys.* **14**, 103020 (2012).
- [21] T. Nishimura, O. Nakatsuka, S. Akimoto, W. Takeuchi, and S. Zaima, *Microelectron. Eng.* **88**, 605 (2011).
- [22] W. Zhu, H. H. Weitering, E. G. Wang, E. Kaxiras, and Z. Zhang, *Phys. Rev. Lett.* **93**, 126102 (2004).
- [23] D. H. Day and R. N. Sinclair, *Acta Crystallogr., Sect. B: Struct. Sci.* **26**, 2079 (1970).
- [24] E. Callen, Y. J. Liu, and J. R. Cullen, *Phys. Rev. B* **16**, 263 (1977).
- [25] M. J. Correia, W. Figueiredo, and W. Schwarzacher, *Phys. Lett. A* **378**, 3366 (2014).
- [26] X. Liu and J. K. Furdyna, *J. Phys.: Condens. Matter* **18**, R245 (2006).
- [27] X. Liu, Y. Sasaki, and J. K. Furdyna, *Phys. Rev. B* **67**, 205204 (2003).
- [28] X. Liu, W. L. Lim, L. V. Titova, M. Dobrowolska, J. K. Furdyna, M. Kutrowski, and T. Wojtowicz, *J. Appl. Phys.* **98**, 063904 (2005).
- [29] Y. Y. Zhou, X. Liu, J. K. Furdyna, M. A. Scarpulla, and O. D. Dubon, *Phys. Rev. B* **80**, 224403 (2009).
- [30] N. Akulov, *Z. Phys.* **100**, 197 (1936).
- [31] C. Zener, *Phys. Rev.* **96**, 1335 (1954).
- [32] S. Chikazumi, *Physics of Magnetism* (Wiley, New York, 1964), Chap. 12.
- [33] W. J. Carr, *J. Appl. Phys.* **29**, 436 (1958).
- [34] W. J. Carr, *Phys. Rev.* **109**, 1971 (1958).
- [35] Y. Fu, I. Barsukov, R. Meckenstock, J. Lindner, Y. Zhai, B. Hjörvarsson, and M. Farle, *J. Appl. Phys.* **115**, 172605 (2014).
- [36] O. N. Mryasov, U. Nowak, K. Y. Guslienko, and R. W. Chantrell, *Europhys. Lett.* **69**, 805 (2005).
- [37] J. B. Staunton, S. Ostanin, S. S. A. Razee, B. L. Gyorffy, L. Szunyogh, B. Ginatempo, and E. Bruno, *Phys. Rev. Lett.* **93**, 257204 (2004).
- [38] J. B. Staunton, L. Szunyogh, A. Buruzs, B. L. Gyorffy, S. Ostanin, and L. Udvardi, *Phys. Rev. B* **74**, 144411 (2006).